

## Early Response Prediction for H<sub>2</sub> Sensors

Raduan Sarif 

Bundesanstalt für Materialforschung und -prüfung (BAM)  
Berlin, Germany  
e-mail: raduan.sarif@bam.de

Carlo Tiebe

Bundesanstalt für Materialforschung und -prüfung (BAM)  
Berlin, Germany  
e-mail: carlo.tiebe@bam.de

Christian Herglotz

Brandenburgische Technische Universität Cottbus-Senftenberg  
Cottbus, Germany  
e-mail: christian.herglotz@b-tu.de

**Abstract**—Green hydrogen (H<sub>2</sub>) is essential for the global transition to clean energy; it will significantly reduce emissions from heavy industry and the long-distance transport system. H<sub>2</sub> can be used as fuel in fuel cells, storing surplus renewable energy, and as a feedstock in industrial processes. However, H<sub>2</sub> faces significant safety challenges during storage and transportation. Accidents due to H<sub>2</sub> leakage and explosions raise serious concerns due to its high flammability, rapid diffusion in air, and extremely low ignition energy. To mitigate risks associated with H<sub>2</sub> leakages, reliable and automated H<sub>2</sub> safety systems are essential for emergency repairs or shutdown. An early response from H<sub>2</sub> sensors is crucial for early warning in accidents. The earlier response time of H<sub>2</sub> sensors is often constrained by their sensor principle, which is heavily influenced by the sensor material's properties. This study explores methods for earlier sensor response through predictive algorithms. Specifically, we investigate transient response predictions using a First-Order (FO) model and propose improvements through the First-Order with early response and the First-Order with adapted early response model. Both models can predict the stable value of the H<sub>2</sub> sensor response from a small time window, which is 70.89% and 83.72% earlier, respectively, than the time required for the sensor hardware to reach it physically. The model's performance is evaluated by calculating the fitting error with a 2 % threshold. Our current research lays the groundwork for future advancements in real-time sensor response predictions for hydrogen leakage.

**Keywords**—H<sub>2</sub> Safety; H<sub>2</sub> Leakage Detection; H<sub>2</sub> Sensor Data Analysis; H<sub>2</sub> Sensor Response Predictions; First-Order (FO) Model.

### I. INTRODUCTION

Hydrogen is crucial for clean energy [1], but storage and transportation are complicated and costly. Two common issues during hydrogen storage and transport are leakage and permeation. Leakage occurs when hydrogen escapes from a container, system, or pipeline due to flaws, holes, or cracks, where the lower flammability limit is a concentration of 4 volume fractions in Vol-% [2]. On the other hand, permeation refers to hydrogen's diffusion through the material walls or interstices of containers, piping, or interface materials [3]. According to [4], the recommended allowable hydrogen permeation rate for new containers tested at 15°C is 6.0 mL/hr/L for passenger cars and 3.7 mL/hr/L for city buses. Based on the permissible permeation rate for passenger cars, the hydrogen permeation from a 5-liter cylinder would correspond to 0.6 Vol% per hour.

The safety concerns associated with hydrogen are due to

the molecule's small size, which makes it particularly prone to leakage [5]. High-pressure hydrogen storage exacerbates the consequences of leakage, leading to higher release flow rates and easier ignition. Notably, hydrogen-related accidents have occurred in various industrial areas. Significant incidents, such as a 2022 refinery fire caused by a hydrogen leak, are of concern for critical safety issues [6]. Thus, intelligent sensor systems are essential for early-stage leakage detection to prevent H<sub>2</sub> related accidents.

Exploiting signal processing methods for sensor responses enables fast and accurate H<sub>2</sub> leakage identification, leveraging transient signals to ensure early response [7]. Although the internal structure of the sensor imposes limitations on its performance, advanced algorithms can significantly improve accuracy and response time. Predicting stable sensor responses from early response accelerates monitoring, reducing the time to detect leaks and improving H<sub>2</sub> safety. Various studies discuss algorithm developments for predicting hydrogen response, such as Osorio-Arrieta et al. [8], applying the Gauss-Newton method to shorten measurement time by fitting the transient response curve. Hübert et al. [9] measured the sensor  $t_{90}$  value based on a mathematical model. Shi et al. [10] use  $SnO_2$ -based sensor response prediction for hydrogen detection by artificial intelligence techniques. After reviewing the above studies, we found that most approaches only approximate the entire sensor response from the sensor's entire response. Additionally, few studies have shown the potential to predict H<sub>2</sub> stable concentration from a small time window of the early response [11]–[13]. Our study explores the H<sub>2</sub> stable concentration and the entire H<sub>2</sub> sensor response using a small time window from the early sensor signal. We also tested the model with different ranges of small time window values, rather than only a specific early sensor response signal. Our current research explores the mathematical feasibility of predicting sensor stable response and  $t_{90}$  values from the early response small time window.

This paper presents a novel method to obtain stable sensor response predictions using an approximation algorithm. Our proposed models use a small time window from the early response of the sensor to predict the entire H<sub>2</sub> sensor response. The structure of this paper is as follows: Section II discusses the H<sub>2</sub> sensor response dynamics and provides a mathematical

explanation of the sensor behavior. Section III describes the experimental setup. Section IV presents the proposed methods, while Section V focuses on the evaluation. Section VI covers the validation, and Section VII provides a detailed discussion. Finally, Section VIII concludes the paper and includes references.

## II. SENSOR RESPONSE DYNAMICS

H<sub>2</sub> sensors are essential to ensure H<sub>2</sub> safety, leak detections, and control and monitoring of H<sub>2</sub> systems. Various H<sub>2</sub> sensors are commercially available [14], exploiting different detection principles such as catalytic combustion, electrochemical reactions, thermal conductivity, and changes in electrical resistivity. Key sensor selection criteria for H<sub>2</sub> safety and monitoring include sensitivity and quick response time [15]. The sensor detection principle, along with the H<sub>2</sub> flow rate and the chamber size, can significantly affect and disrupt the response time.

Boon-Brett et al. [16] discuss the different methods and setups that affect response time. Sensor response dynamics can be categorized as extrinsic or intrinsic. The extrinsic response time involves gas delivery dynamics influenced by measurement chamber volume and the H<sub>2</sub> flow rates. The intrinsic response time is related to the physical properties of the sensor, reflecting the delay between the exposure of H<sub>2</sub> to the sensing element and the first detection of the signal, known as deadtime  $\theta$  (seconds).

A graphical representation of an exemplary H<sub>2</sub> concentration (volume fraction in Vol-%) in a chamber is shown in Figure 1. The green curve represents an exponential sensor response with both H<sub>2</sub> increasing and decreasing concentrations for 9600 seconds. With a First Order (FO) model, we can approximate the idealized sensor's response (red curve) for 7200 seconds. Also, the step function (blue curve) defines the release of H<sub>2</sub> flow. H<sub>2</sub> was released at -200 seconds, but the sensor began responding at 0 seconds, which is defined as the deadtime. The maximum sensor response is 0.8 volume fraction in Vol-%.  $t_{90}$  represents the time at which the sensor's output reaches 90% of its stable value. In this case,  $t_{90}$  is 775 seconds for a concentration of 0.72 Vol-%.

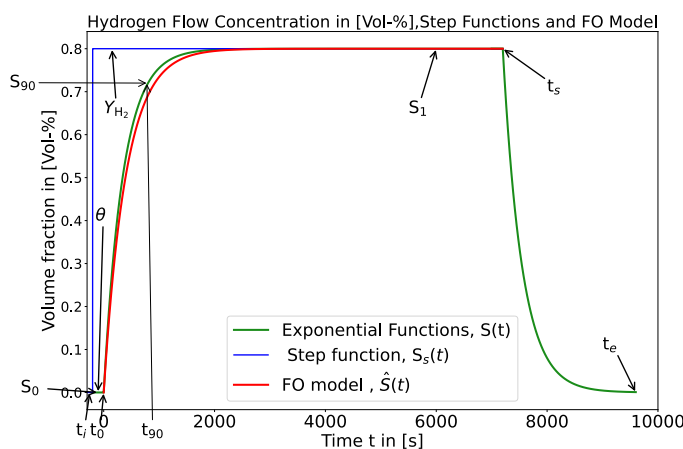


Figure 1: Visualization of exponential functions, step function and FO model for H<sub>2</sub> flow concentration (Vol-%).

As stated in the literature [17], the sensor element transfer function and the transient gas sensor response signal can be modeled as an exponential function. This approach allows determining the transient response curve of the hydrogen sensor for a specified concentration (volume fraction in Vol %) [17]. With changing H<sub>2</sub> concentration, exponential functions can describe both the increase and decrease of the H<sub>2</sub> sensor response.

The sensor response can be idealized by using exponential functions. Equation (1) describes the ideal response  $S(t)$ , which consists of three exponential functions for changing concentrations over time  $t$  (seconds). The time state  $t_i$  (seconds) indicates the H<sub>2</sub> concentration release time and also the time of the first recorded measured sample.  $t_0$  (seconds) denotes the moment when the sensor starts to react in H<sub>2</sub> flow changing. The time  $t_s$  (seconds) is assumed to be the time at which the sensor reaches its maximum stable response, while  $t_e$  (seconds) represents the time at which the sensor reaches its lowest stable response. Three distinct cases are described below:

- 1) **No Reaction (Deadtime):** No sensor reaction over H<sub>2</sub> flow changes for the period of  $t_i \leq t < t_0$ . This duration is called deadtime  $\theta$ , where the sensor does not yet detect the presence of H<sub>2</sub>. After this delay, the sensor begins to register its first response.
- 2) **Transient Increasing Response:** During  $t_0 \leq t \leq t_s$ , the sensor starts to react to the presence of H<sub>2</sub> concentration. The response increases as the sensor detects and records the H<sub>2</sub> concentration. We assume that the sensor reaches a maximum stable response at  $t_s$  seconds, where we stop the H<sub>2</sub> release.
- 3) **Transient Decreasing Response:** In the final phase, for  $t_s \leq t < t_e$ , the sensor response decreases as the H<sub>2</sub> concentration decreases inside the chamber. The decreasing response is recorded until it reaches the lowest stable sensor value, which we assume occurs at  $t_e$  seconds.

$$S(t) = \begin{cases} S_0, & t_i \leq t < t_0 \\ S_1 \cdot \left(1 - e^{-\frac{t-t_0}{\tau}}\right), & t_0 \leq t \leq t_s \\ S_1 \cdot e^{-\frac{(t-t_s)}{\tau}}, & t_s \leq t < t_e \end{cases} \quad (1)$$

Summarizing, the entire sensor response can be described by  $S(t)$ , where  $S_0$  is a constant representing the sensor response before H<sub>2</sub> release, whose value should be zero.  $S_1$  is the stable sensor response signal after H<sub>2</sub> flow change. Time constant  $\tau$  is defined as the ratio of the chamber volume  $V$  in the unit liter (L) to the hydrogen flow rate  $\dot{V}_{H_2}$  in the unit liter per minute (L/min) in (2).

$$\tau = \frac{V}{\dot{V}_{H_2}} \quad (2)$$

Equation (3) presents the step functions  $S_s(t)$  for H<sub>2</sub> flow  $Y_{H_2}$  changes. Before time  $t_i$ , there is a 0% H<sub>2</sub> flow, after  $t_i$ , there is a H<sub>2</sub> flow  $Y_{H_2}$  upto time  $t_s$ .

$$S_s(t) = \begin{cases} 0, & t \leq t_i \\ Y_{H_2}, & t_i \leq t \leq t_s \end{cases} \quad (3)$$

The sensor's increasing and decreasing response characteristics, including response time and the  $t_{90}$  time, are essential for ensuring  $H_2$  safety. ISO 26142 defines response time as the interval from  $H_2$  exposure until the sensor reaches a stable output, which corresponds to the duration of  $t_0 \leq t \leq t_s$  in (1). The  $t_{90}$  time is the time for the sensor value to reach 90% of maximum stable response [18]. The  $t_{90}$  time is crucial for early leak detection and should be minimized to prevent accidents.

Equation (4) calculates the theoretical  $t_{90}$  (seconds) time for  $H_2$  sensors. The sensor response value should match the  $t_{90}$  time derived from (4) to be considered a stable response, which is the inverse function of (1) case 2.

$$t_{90} = -\ln\left(1 - \frac{S_{90}}{S_1}\right) \tau \quad (4)$$

In the previous parts, we provided the theoretical background of ideal sensor responses, which can be approximated using various mathematical process modeling approaches. Among them, the First Order Plus Dead Time (FOPDT) model is widely used for simplifying process dynamics, particularly in feedback control loop design [19]. This model is the baseline to construct our simplification, where we focus on the sensor response increasing curve,  $t$ , in the range  $t_0 \leq t \leq t_s$ . Furthermore, we simplify the FOPDT to the First Order (FO) model, considering the deadtime  $\theta$  equal to zero. Equation (5) presents the FOPDT model from [20] and FO model in (6), where  $\hat{S}$  represents the estimated sensor response.

$$\tau \frac{d\hat{S}}{dt} + \hat{S}(t) = K \cdot S_s(t - \theta) \quad (5)$$

$$\tau \frac{d\hat{S}}{dt} + \hat{S}(t) = K \cdot S_s(t) \quad (6)$$

The steady-state gain ( $K$ ) is the ratio of the sensor's response signal corresponding to a step input, as defined in (7).

$$K = \frac{S_1}{Y_{H_2}} \quad (7)$$

Equation (6) replaces the value of ( $K$ ) and  $S_s(t)$  from (7) and (3). The revised model is presented in (8).

$$\tau \frac{d\hat{S}}{dt} + \hat{S}(t) = S_1 \quad (8)$$

In addition, the transfer function of the FO (Laplace transformation of (6)) is described by (9), which is commonly used to approximate processes. This study will use this equation to predict the  $H_2$  sensor response based on a small time window from the early response of the sensor.

$$\hat{S}(t) = S_1 \cdot \left(1 - e^{-\frac{t}{\tau}}\right) \quad (9)$$

### III. EXPERIMENTAL SETUP

This experiment used the NEO983 sensor with a  $H_2$  detection threshold of less than 0.15 volume fraction in Vol-% and a response time of under 3 seconds and  $t_{90}$  time of less than 5 seconds. The sensor was tested in a measurement chamber using a double cross-piece DN 160 ISO-K chamber [21].  $H_2$  was mixed with air during the experiment to create the desired concentration, where airflow volume fractions were 99.2 volume fraction in Vol-%, and  $H_2$  volume fraction was 0.8 volume fraction in Vol-%. The airflow rate was 992 mL/min, and the  $H_2$  flow rate was adjusted to 8 mL/min. Therefore, with a gas flow rate of 1000 mL/min and a chamber volume of 5.8 L. Based on (2), the time constant ( $\tau$ ) is 348 seconds, resulting in a calculated  $t_{90}$  time of 801 seconds based on (4).

This setup provided a stable and well-mixed environment for evaluating the sensor's performance under specific  $H_2$  concentrations. The experiment was conducted over two hours following the release of  $H_2$ . Once the sensor recorded a stable response, the  $H_2$  release was stopped; after that, the sensor response was monitored until it declined to zero. The NEO983 sensor detected a maximum  $H_2$  concentration of 0.75 volume fraction in Vol-%, compared to the released concentration of 0.8 volume fraction in Vol-%. Figure 2 illustrates the Piping and Instrumentation Diagram (P&ID), a detailed schematic that illustrates the experimental process's piping, equipment, and instrumentation, showing how components are interconnected and controlled. The overall gas flow setup includes a control valve, Mass Flow Controller (MFC), and gas mixer to accurately regulate, measure, and mix  $H_2$  gases.

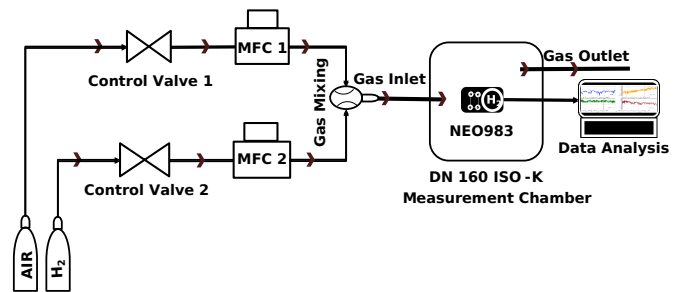


Figure 2: Experiment Pipe & Instrumentation Design.

An additional experiment was conducted as reported in [22], using  $H_2$  concentrations of 0.5, 1.0, 1.5, 2.0, 2.5, 3.0, 3.5, and 4.0 Vol-%. Using the same chamber volume, the gas flow rate is 4643 mL/min with a flow uncertainty of  $\pm 65.8$  mL/min. In this case, the time constant ( $\tau$ ) is 75 seconds based on (2), and according to (4), the corresponding calculated  $t_{90}$  time is 173 seconds. The sensor response for each concentration was recorded over two hours to observe stable values. These datasets are used for validation in our study. Data analysis and model predictions were performed using the Python programming language within the Jupyter Notebook environment [23].

### IV. METHODS

In this research, our goal is to rapidly estimate the  $H_2$  sensor response using a small time window from the early response

of the sensor. We aim to minimize the prediction time  $\hat{t}$ , which is passed until a reliable estimate of the sensor response is available, while ensuring a low fitting error in the predicted response  $\hat{S}(t)$ .

We propose three approaches based on the First-Order (FO) model to achieve the research objective. First, we use the real sensor response data to approximate the entire sensor response. Here,  $S_r(t)$  is the time series from a real sensor response, and the variable  $t$  is used as a discrete-time index. Next, we define a small time window value  $S_w(t)$  to predict the sensor response.  $S_w(t)$  begins at the time index corresponding to a threshold value  $S_{th} > 0$  Vol-% and ends at time instance  $t_w$ . In the last step, we adapt the  $S_{th}$  values to improve performance. Finally, the total prediction time  $\hat{t}$  is obtained by summing  $t_w$  and the model processing time  $t_m$ , as shown in (10). The model processing time  $t_m$ , represents the calculation time to predict  $\hat{S}(t)$  from small time window value  $S_w(t)$ .

$$\hat{t} = t_m + t_w \quad (10)$$

All three models' outcomes, corresponding fitting errors, and model time-saving efficiency are presented in Section V.

#### A. FO with Baseline (FOB)

FOB is the baseline model in this study to predict the sensor response  $\hat{S}(t)$  from the real sensor response  $S_r(t)$ . This FOB model took  $S_r(t)$  within time range  $t_0 \leq t \leq t_s$  as an input to predict the  $\hat{S}(t)$ . Figure 3 illustrates the sensor response  $S_r(t)$  (green curve) with time on the x-axis (in seconds) and  $H_2$  concentration (volume fraction in Vol-%) on the y-axis. The sensor response stable value was 0.75 volume fraction in Vol-%,  $t_{90}$  recorded at 1131 seconds with the  $S_{90}$  of 0.68 volume fraction in Vol-%. Finally, the sensor response was approximated using the FOB (red curve), where  $\hat{S}(t)$  has a stable value of 0.75 Vol-%.

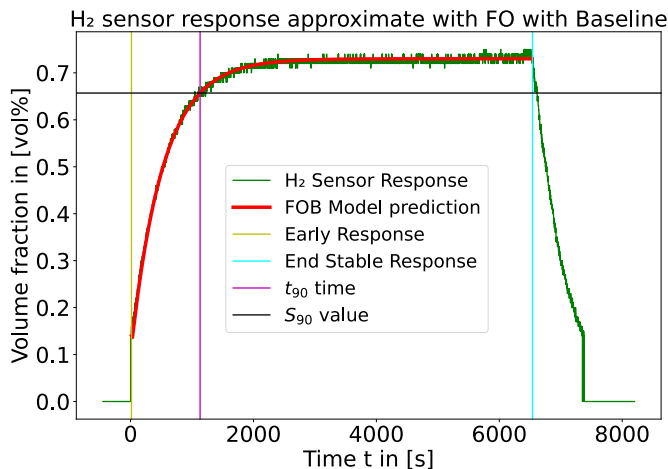


Figure 3: Sensor measure value (green) fitted with FO in Baseline (red).

#### B. FO with Early Response (FOER)

In FOER, we aim to fit the model to predict the sensor response  $\hat{S}(t)$  from a small time window value  $S_w(t)$ .  $S_w(t)$

starts from the time when the sensor response is greater than 0 Vol-% and continues until time  $t_w$ . Therefore, the FOER model sets the threshold  $S_{th} > 0$  Vol-%. Figure 4 illustrates the  $S_w(t)$  (blue curve), where the time window  $t_w = 535$ s. The predicted sensor response  $\hat{S}(t)$  is the red curve with the stable value of 0.75 Vol-%, while the real sensor response  $S_r(t)$  is in green curve with the stable value of 0.75 Vol-%. As  $t_m$  is 1s, based on (10) the estimation time  $\hat{t}$  is 536 seconds.

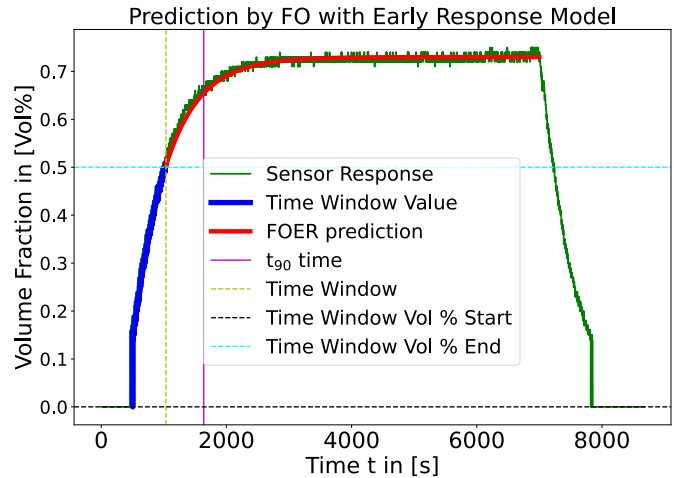


Figure 4: Prediction by FO with early response model.

#### C. FO with Adapted Early Response (FOAER)

In FOAER, an adapted early response method predicts  $\hat{S}(t)$  from  $S_w(t)$  by considering a higher  $S_{th}$  rather than 0 Vol-%. As a result, we expect that FOAER requires a smaller time window because the impact of the step when the sensor first reacts to the  $H_2$  is mitigated.

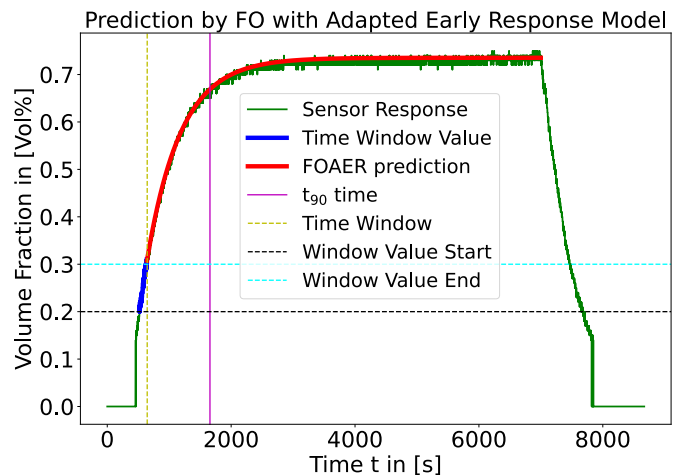


Figure 5: Prediction by FO with adapted early response.

With a threshold of  $S_{th} = 0.20$  Vol-%, the model predicts a stable response value of  $\hat{S}(t) = 0.74$  Vol-% (red curve), where real sensor's stable value of  $S_r(t) = 0.75$  Vol-% (green curve), as shown in Figure 5. Also, Figure 5 depicts  $S_w(t)$  in

blue curve, where the time window ends at  $t_w = 121$  seconds. Based on (10),  $\hat{t} = 122$  seconds, where  $t_m = 1$ s.

## V. EVALUATION

We evaluate the overall fitting accuracy by calculating the relative fitting error  $\varepsilon$  in (11). The error is computed between the real sensor response  $S_r(t)$  and the model estimation  $\hat{S}(t)$ . The error is computed over discrete time indices  $t_i$ , where  $t_0 \leq t_i \leq t_s$ , and the total number of index samples is  $N$ . The final  $\varepsilon$  is calculated by summing the errors of  $N$  samples and dividing by the number of samples  $N$ .

$$\varepsilon = \frac{1}{N} \sum_{i=1}^N \left( \frac{|S_r(t_i) - \hat{S}(t_i)|}{S_r(t_i)} \right) \times 100\% \quad (11)$$

Figure 6 illustrates the relationship between the fitting error ( $\varepsilon$ ) and estimated time  $\hat{t}$  for the FOER (blue) and the FOAER (orange). The minimum fitting error ( $\varepsilon$ ) over  $\hat{t}$  is 0.74% for the FOER and 0.76% for the FOAER. By considering the dynamic behavior of the sensor, this research considers a model error threshold  $\leq 2\%$  as an acceptable and sufficiently good fit. For both our models, fitting error ( $\varepsilon$ ) was below the threshold of  $\leq 2\%$ .

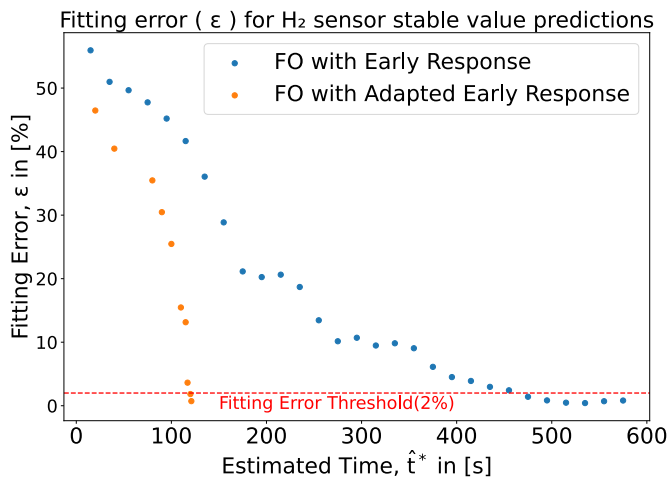


Figure 6: Fitting error (%) for FOER and FOAER.

The main objective of this research is to estimate stable values as quickly as possible. To evaluate this, we calculate the relative time savings  $\eta_s$  by comparing models' estimation time ( $\hat{t}^*$ ) with the sensor's response ( $t_{90}$ ) defined in (12). The  $\hat{t}^*$  is the estimation time corresponding to the minimum fitting error, when the error remains below the 2% threshold. The  $t_{90}$  is crucial because it is a common metric to indicate the detection time in the literature [17]. In this study, the sensor response ( $t_{90}$ ) time was obtained through graphical analysis. If the value  $\eta_s$  is higher, this indicates that the model's prediction efficiency is good and requires less time to predict stable values.

$$\eta_s = \left( \frac{t_{90} - \hat{t}^*}{t_{90}} \right) \times 100\% \quad (12)$$

For estimation time  $\hat{t}^*$  the FOER model,  $\eta_s$  is 70.89%, while for the FOAER model, it is 84.50%. Hence, using the FOAER model, we can predict the stable value 13.51% faster than the FOER model.

## VI. VALIDATION

In Figure 7 (for FOER) and Figure 8 (for FOAER), we have presented the scatter plots of the fitting errors ( $\varepsilon$ ) over estimations time  $\hat{t}^*$ , which include  $H_2$  concentrations of 0.5 (blue), 1.0 (orange), 1.5 (green), 2.0 (red), 2.5 (purple), 3.0 (brown), 3.5 (pink), and 4.0 (gray) Vol%. For each concentration, we have considered individual estimation times  $\hat{t}^*$  corresponding to the minimum fitting error ( $\varepsilon$ ).

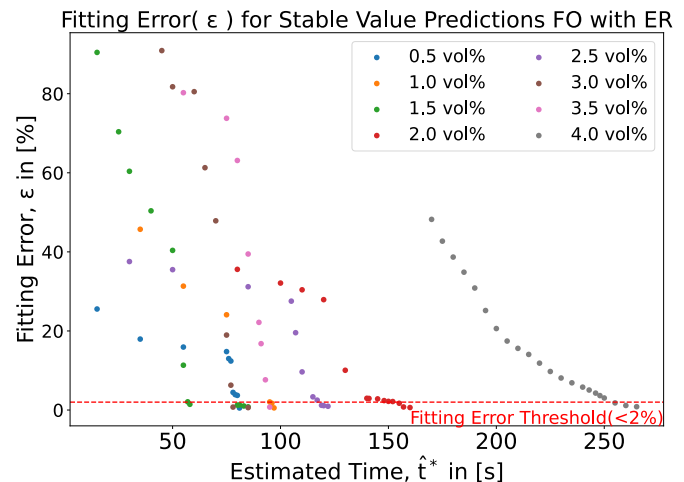


Figure 7: Fitting error ( $\varepsilon$ ) for FOER.

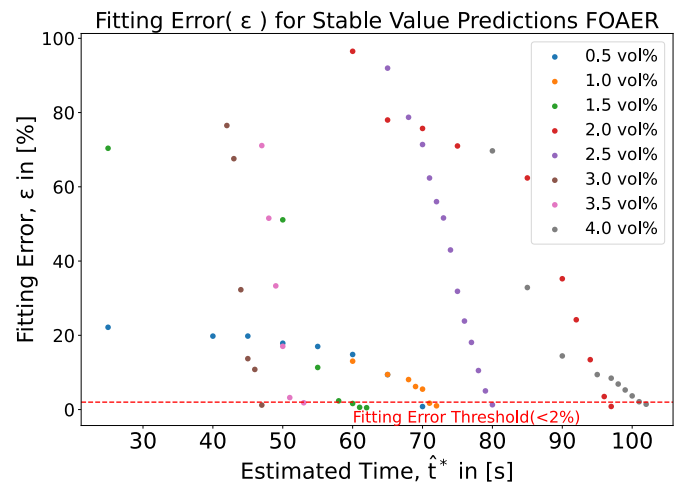


Figure 8: Fitting error ( $\varepsilon$ ) for FOAER.

Table I and Table II present a summary of the  $H_2$  concentration flow, sensor response, and prediction results for the FOER and FOAER models, respectively. Both tables' values in the first and second columns show the target  $H_2$  concentration (Vol%) starting and ending values, which are defined as  $Q_s$  and  $Q_e$ . The third column shows the sensor's  $t_{90}$  response time, followed by the model's estimated time in the fourth column.

The fifth column presents the calculated relative time saved by the model compared to the sensor's  $t_{90}$  time. The sixth and seventh columns list the real stable sensor response and the model-predicted stable value, respectively. Finally, the seventh column reports the fitting error between the model and the real sensor stable values. The FOAER models included the adaptive threshold values in the last column of the table.

TABLE I: FOER MODEL SUMMARY:  $Q_s, Q_e$  – START/END  $H_2$  CONCENTRATIONS (VOL-%);  $t_{90}, \hat{t}^*$  – SENSOR/MODEL TIMES (S);  $\eta_s, \varepsilon$  – TIME SAVING/ERROR (%);  $S_r(t), \hat{S}(t)$  – REAL/PREDICTED RESPONSES (VOL-%);  $\mu$  – MEAN.

$Q_s$	$Q_e$	$t_{90}$	$\hat{t}^*$	$\eta_s$	$S_r(t)$	$\hat{S}(t)$	$\varepsilon$
0.0	0.8	1131	536	73.20	0.75	0.75	0.74
0.0	0.5	396	82	79.04	0.46	0.46	0.52
0.5	1.0	434	98	77.42	0.95	0.95	0.56
1.0	1.5	436	86	80.28	1.45	1.45	0.85
1.5	2.0	435	161	62.99	1.95	1.95	0.63
2.0	2.5	431	123	71.93	2.45	2.45	0.96
2.5	3.0	418	86	79.43	2.92	2.92	0.64
3.0	3.5	411	96	76.64	3.42	3.42	0.76
3.5	4.0	423	266	37.12	3.93	3.93	0.87
$\mu$	-	-	170.44	70.89	-	-	0.73

TABLE II: OVERVIEW OF FOAER:  $Q_s, Q_e$  – START/END  $H_2$  CONCENTRATIONS (VOL-%);  $t_{90}, \hat{t}^*$  – SENSOR/MODEL TIMES (S);  $\eta_s, \varepsilon$  – TIME SAVING/ERROR (%);  $S_r(t), \hat{S}(t), S_{th}$  – RESPONSES/THRESHOLD (VOL-%);  $\mu$  – MEAN.

$Q_s$	$Q_e$	$t_{90}$	$\hat{t}^*$	$\eta_s$	$S_r(t)$	$\hat{S}(t)$	$\varepsilon$	$S_{th}$
0.0	0.8	1131	122	84.50	0.75	0.75	0.76	0.20
0.0	0.5	396	71	82.07	0.46	0.46	0.84	0.10
0.5	1.0	434	72	83.41	0.95	0.95	1.00	0.24
1.0	1.5	436	63	85.55	1.45	1.45	0.56	0.10
1.5	2.0	435	98	77.47	1.95	1.94	0.87	0.29
2.0	2.5	431	82	80.97	2.45	2.44	1.29	0.35
2.5	3.0	418	81	88.04	2.92	2.91	1.22	0.40
3.0	3.5	411	54	86.86	3.42	3.43	1.83	0.43
3.5	4.0	423	104	75.41	3.93	3.94	1.45	0.55
$\mu$	-	-	79.33	83.72	-	-	1.09	0.30

In the tables above, the mean ( $\mu$ ) for all samples was calculated using (13), where  $y_i$  denotes each sample value and  $n$  is the total number of samples:

$$\mu = \frac{1}{n} \sum_{i=1}^n y_i \quad (13)$$

The computed mean values for estimation time, fitting error, relative time saving, and adaptive threshold are shown in the last row of both tables.

## VII. DISCUSSION

We performed a two-sample t-test [24] to statistically evaluate the similarity in the estimation times  $\hat{t}^*$  of the FOER and FOAER models. The test provides a  $t$ -value, which determines the difference in the variability in the data, and a  $p$ -value, which indicates the probability that the observed difference occurred by chance. If the critical  $t$ -value 2.306 for  $p = 0.05$ , as listed in the t-distribution tables [25] is greater than the calculated  $t$ -value, the result is considered not statistically

significant, indicating that no strong evidence exists to conclude a significant difference between the models.

The model estimation times  $\hat{t}^*$  cannot be directly compared because the experiments were conducted under two different time constants ( $\tau$ ). To enable a meaningful comparison and perform a  $t$ -test, the estimation time at 0.8 vol% was compensated to align with the conditions used for concentrations from 0.5 to 4.0 vol%, based on (14). Here,  $\hat{t}_1^*$  represents the model estimation time obtained at 0.8 vol% with a time constant of  $\tau_1 = 348$  seconds, and it is adjusted to  $\hat{t}_2^*$ , corresponding to  $\tau_2 = 75$  seconds, which was used for the concentrations 0.5 to 4.0 vol%. As a result, for 0.8 vol% the compensated estimation times are  $\hat{t}_2^* = 118$  s for the FOER model and  $\hat{t}_2^* = 26.84$  s for the FOAER model.

$$\hat{t}_2^* = \hat{t}_1^* \cdot \frac{\tau_2}{\tau_1} \quad (14)$$

As shown in Table I and Table II, the estimation time ( $\hat{t}^*$ ) for the FOER model has a mean of 170.44 seconds, while the FOAER model has a mean of 79.33 seconds. After compensating 0.8 vol% estimation time ( $\hat{t}^*$ ), the FOER model has a mean of 123.67 s with a standard deviation of 54.83 s, while the FOAER model has a mean of 68.92 s and a standard deviation of 22.38 s. Based on a two-sample  $t$ -test, the calculated  $t$ -value is 2.59, which is greater than the critical  $t$ -value of 2.306 at a significance level of  $p = 0.05$ , as referenced in the t-distribution tables [25]. Since the calculated  $t$ -value is greater than the critical threshold, we conclude that there is a statistically significant difference between the estimation times of the FOER and FOAER models. However, when excluding the values corresponding to 0.8 vol%, the  $t$ -value drops to 2.18, below the critical  $t$ -value. This indicates no statistically significant difference between the estimation times of the two models. The  $t$ -test results suggest that both models predict the sensor response independently, but their prediction performance is strongly correlated with the time constant ( $\tau$ ) and the extrinsic response time.

Overall, the FOER model achieves an average time-saving efficiency of 70.89% with a fitting error of 0.73%, using a fixed threshold  $S_{th} > 0$ . In comparison, the FOAER model shows an average higher time-saving efficiency of 83.72% and a fitting error of 1.09%, with the mean threshold of  $S_{th} = 0.30$  Vol%. Both models can predict the sensor response using data from a small time window; however, the FOAER model is more appropriate for  $H_2$  leakage detection.

## VIII. CONCLUSION

The study aims to predict the sensor response from a small time window of the sensor's early response without waiting for the sensor values to converge. By leveraging sensor data from various  $H_2$  concentration responses, two FO model approaches are used to make accurate predictions. The evaluation of the models was calculated by the average fitting error (%) with a  $< 2\%$  threshold and model prediction efficiency. We find that the stable value of the sensor can be predicted in the transient phase of the sensor response with an average fitting error of 0.73%

(for FOER) and 1.09% (for FOAER). This approach allows the detection rate of dangerous concentrations of H<sub>2</sub> 70.89 % and 83.72 % earlier than naive methods using unprocessed sensor data. The advantage of the FO model is that it captures systems with exponential response behavior and offers a simple, interpretable framework that requires minimal data, making it well-suited for processes with known dynamics. But on the other hand, data-driven models—such as neural networks or regression techniques—learn input-output relationships from large datasets without relying on a physical model, enabling them to predict sensor responses independently of system-specific dynamics. While this study focused on a single sensor with a deterministic response using the FO model, future work will expand the experimental setup to include multiple sensors and environmental factors, such as temperature and pressure. This will allow the application of data-driven models to capture the system's complexity and variability. Additionally, uncertainties in sensor responses will be addressed to generate large-scale datasets for training robust multivariate data analysis models that can accurately predict sensor stable responses.

Finally, to integrate our approach into embedded sensor systems or edge computing environments, we will develop software that incorporates the trained prediction model and interfaces with the sensor system. In practical applications, this software will capture the H<sub>2</sub> sensor's early response signal immediately after gas exposure, within a defined time window. The model will then analyze this early response to estimate the sensor's stable output value, enabling the system to make rapid decisions or transmit the predicted concentration to a user interface or cloud platform. This approach supports real-time predicting potentially explosive H<sub>2</sub> leaks in critical environments such as hydrogen refueling stations or pipelines. The predicted value will be continuously compared against a predefined explosion threshold to trigger timely warnings, activate alarms, or initiate automatic safety shutdowns when necessary.

#### REFERENCES

- [1] Q. Hassan, S. Algburi, A. Z. Sameen, H. M. Salman, and M. Jaszczur, "Green hydrogen: A pathway to a sustainable energy future", *International Journal of Hydrogen Energy*, vol. 50, pp. 310–333, 2024.
- [2] M. Molnarne and V. Schroeder, "Hazardous properties of hydrogen and hydrogen containing fuel gases", *Process Safety and Environmental Protection*, vol. 130, pp. 1–5, 2019.
- [3] W. Umrath, *Fundamentals of Vacuum Technology*. Leybold GmbH, Cologne, 2016, Accessed: July, 01, 2025.
- [4] P. Adams, A. Bengaouer, B. Cariteau, V. Molkov, and A. Venetsanos, "Allowable hydrogen permeation rate from road vehicles", *International Journal of Hydrogen Energy*, vol. 36, no. 3, pp. 2742–2749, 2011.
- [5] L. Guo *et al.*, "Hydrogen safety: An obstacle that must be overcome on the road towards future hydrogen economy", *International Journal of Hydrogen Energy*, vol. 51, pp. 1055–1078, 2024.
- [6] J. X. Wen *et al.*, "Statistics, lessons learned and recommendations from analysis of hiad 2.0 database", *International journal of hydrogen energy*, vol. 47, no. 38, pp. 17 082–17 096, 2022.
- [7] R. R. Patil, R. K. Calay, M. Y. Mustafa, and S. Thakur, "Artificial intelligence-driven innovations in hydrogen safety", *Hydrogen*, vol. 5, no. 2, pp. 312–326, 2024.
- [8] D. L. Osorio-Arrieta *et al.*, "Reduction of the measurement time by the prediction of the steady-state response for quartz crystal microbalance gas sensors", *Sensors*, vol. 18, no. 8, p. 2475, 2018.
- [9] T. Hübert, J. Majewski, U. Banach, M. Detjens, and C. Tiebe, "Response time measurement of hydrogen sensors", *Hydrogen Knowledge Centre*, 2017.
- [10] C. Shi, W. Pei, C. Jin, A. Alizadeh, and A. Ghanbari, "Prediction of the sno2-based sensor response for hydrogen detection by artificial intelligence techniques", *International Journal of Hydrogen Energy*, vol. 48, no. 52, pp. 19 834–19 845, 2023.
- [11] Y. Shi, S. Ye, and Y. Zheng, "Rapid forecasting of hydrogen concentration based on a multilayer cnn-lstm network", *Measurement Science and Technology*, vol. 34, no. 6, p. 065 101, 2023. DOI: 10.1088/1361-6501/acbdb5.
- [12] V. Martvall *et al.*, "Accelerating plasmonic hydrogen sensors for inert gas environments by transformer-based deep learning", *ACS sensors*, 2025.
- [13] R. Yang *et al.*, "Ultrafast hydrogen detection system using vertical thermal conduction structure and neural network prediction algorithm based on sensor response process", *ACS sensors*, vol. 10, no. 3, pp. 2181–2190, 2025.
- [14] European Commission, *bibleothek – A Bible-based Cultural Network*, <https://cordis.europa.eu/project/id/325326>, Project No. 325326, CORDIS: EU Research Results, 2016.
- [15] W. J. Buttner, M. B. Post, R. Burgess, and C. Rivkin, "An overview of hydrogen safety sensors and requirements", *International Journal of Hydrogen Energy*, vol. 36, no. 3, pp. 2462–2470, 2011.
- [16] L. Boon-Brett *et al.*, "Identifying performance gaps in hydrogen safety sensor technology for automotive and stationary applications", *International Journal of Hydrogen Energy*, vol. 35, no. 1, pp. 373–384, 2010.
- [17] T. Hübert and U. Banach, "Response time of hydrogen sensors", in *Proceedings of the Fifth International Conference on Hydrogen Safety*, 2013, pp. 9–11.
- [18] *ISO 26142:2010: Hydrogen detection apparatus – Stationary applications*, Standard, International Organization for Standardization, 2010.
- [19] C. I. Muresan and C. M. Ionescu, "Generalization of the fopdt model for identification and control purposes", *Processes*, vol. 8, no. 6, p. 682, 2020.
- [20] C. Cox, J. Tindle, and K. Burn, "A comparison of software-based approaches to identifying fopdt and sopdt model parameters from process step response data", *Applied Mathematical Modelling*, vol. 40, no. 1, pp. 100–114, 2016.
- [21] Pfeiffer Vacuum GmbH, *Right angle valve, 320rkd160*, <https://www.pfeiffer-vacuum.com/global/en/shop/products/320RKD160>, Accessed: May 30, 2025.
- [22] M. Bayat and C. Tiebe, *Measurement and Testing Methods for Sensors in Hydrogen Technologies*, BAM TF Tag Energie, 2024.
- [23] R. Sarif, "Fopdt model h2 response prediction code", Accessed: July 01, 2025, 2025, [Online]. Available: <https://github.com/Raduan01/H2-Response/blob/main/FOPDT%20model%20H2%20Response%20Prediction%20code.py>.
- [24] NIST/SEMATECH, *1.3.5.2. Confidence Limits for the Mean*, <https://www.itl.nist.gov/div898/handbook/eda/section3/eda352.htm>, NIST/SEMATECH Engineering Statistics Handbook 2012, Accessed: 2025-07-02.
- [25] NIST/SEMATECH, *Engineering statistics handbook 2012-3.6.7.2. paired t-test*, <https://www.itl.nist.gov/div898/handbook/eda/section3/eda3672.htm>, Accessed: May 30, 2025.